Dead zones in colloidal quantum dot photovoltaics: evidence and implications

D. Aaron R. Barkhouse, Illan J. Kramer, Xihua Wang, and Edward H. Sargent*

Department of Electrical and Computer Engineering, University of Toronto,
10 King's College Road, Toronto, Ontario M5S 3G4, Canada
**ted.sargent@utoronto.ca*

Abstract: In order to fabricate photovoltaic (PV) cells incorporating light-trapping electrodes, flexible foil substrates, or more than one junction, illumination through the top-contact (i.e.: non-substrate) side of a photovoltaic device is desirable. We investigate the relative collection efficiency for illumination through the top vs. bottom of PbS colloidal quantum dot (CQD) PV devices. The external quantum efficiency spectra of FTO/TiO_2/PbS CQD/ITO PV devices with various PbS layer thicknesses were measured for illumination through either the top (ITO) or bottom (FTO) contacts. By comparing the relative shapes and intensities of these spectra with those calculated from an estimation of the carrier generation profile and the internal quantum efficiency as a function of distance from the TiO_2 interface in the devices, a substantial dead zone, where carrier extraction is dramatically reduced, is identified near the ITO top contact. The implications for device design, and possible means of avoiding the formation of such a dead zone, are discussed.

OCIS codes: (230.0230) Optical devices; (250.0250) Optoelectronics; (040.5350) Photovoltaic; (250.5590) Quantum-well, -wire and -dot devices.

References and links

1. J. Zhu, Z. F. Yu, G. F. Burkhard, C. M. Hsu, S. T. Connor, Y. Q. Xu, Q. Wang, M. McGehee, S. H. Fan, and Y. Cui, "Optical absorption enhancement in amorphous silicon nanowire and nanocone arrays," Nano Lett. **9**(1), 279–282 (2009).
2. Z. Y. Fan, H. Razavi, J. W. Do, A. Moriwaki, O. Ergen, Y. L. Chueh, P. W. Leu, J. C. Ho, T. Takahashi, L. A. Reichertz, S. Neale, K. Yu, M. Wu, J. W. Ager, and A. Javey, "Three-dimensional nanopillar-array photovoltaics on low-cost and flexible substrates," Nat. Mater. **8**(8), 648–653 (2009).
3. D. Bremaud, D. Rudmann, M. Kaelin, K. Ernits, G. Bilger, M. Dobeli, H. Zogg, and A. N. Tiwari, "Flexible Cu(In,Ga)Se-2 on Al foils and the effects of Al during chemical bath deposition," Thin Solid Films **515**(15), 5857–5861 (2007).
4. X. Mathew, J. P. Enriquez, A. Romeo, and A. N. Tiwari, "CdTe/CdS solar cells on flexible substrates," Sol. Energy **77**(6), 831–838 (2004).
5. A. Romeo, A. Terheggen, D. Abou-Ras, D. L. Batzner, F. J. Haug, M. Kalin, D. Rudmann, and A. N. Tiwari, "Development of thin-film Cu(In,Ga)Se-2 and CdTe solar cells," Prog. Photovoltaics **12**(23), 93–111 (2004).
6. A. G. Pattantyus-Abraham, I. J. Kramer, A. R. Barkhouse, X. Wang, G. Konstantatos, R. Debnath, L. Levina, I. Raabe, M. K. Nazeeruddin, M. Grätzel, and E. H. Sargent, "Depleted-heterojunction colloidal quantum dot solar cells," ACS Nano **4**(6), 3374–3380 (2010).
7. D. A. R. Barkhouse, A. G. Pattantyus-Abraham, L. Levina, and E. H. Sargent, "Thiols passivate recombination centers in colloidal quantum dots leading to enhanced photovoltaic device efficiency," ACS Nano **2**(11), 2356–2362 (2008).
8. J. P. Clifford, G. Konstantatos, K. W. Johnston, S. Hoogland, L. Levina, and E. H. Sargent, "Fast, sensitive and spectrally tuneable colloidal-quantum-dot photodetectors," Nat. Nanotechnol. **4**(1), 40–44 (2009).
9. G. I. Koleilat, L. Levina, H. Shukla, S. H. Myrskog, S. Hinds, A. G. Pattantyus-Abraham, and E. H. Sargent, "Efficient, stable infrared photovoltaics based on solution-cast colloidal quantum dots," ACS Nano **2**(5), 833–840 (2008).
10. J. M. Luther, M. Law, M. C. Beard, Q. Song, M. O. Reese, R. J. Ellingson, and A. J. Nozik, "Schottky solar cells based on colloidal nanocrystal films," Nano Lett. **8**(10), 3488–3492 (2008).
11. M. Law, M. C. Beard, S. Choi, J. M. Luther, M. C. Hanna, and A. J. Nozik, "Determining the internal quantum efficiency of PbSe nanocrystal solar cells with the aid of an optical model," Nano Lett. **8**(11), 3904–3910 (2008).
12. H. Schmidt, H. Flugge, T. Winkler, T. Bulow, T. Riedl, and W. Kowalsky, "Efficient semitransparent inverted organic solar cells with indium tin oxide top electrode," Appl. Phys. Lett. **94**(24), 243302 (2009).

#131000 - $15.00 USD Received 1 Jul 2010; revised 27 Aug 2010; accepted 27 Aug 2010; published 1 Sep 2010

13. K. C. Liu, C. W. Teng, Y. H. Lu, J. H. Lee, and L. C. Chen, "Improving the performance of transparent PLEDs with LiF/Ag/ITO cathode," Electrochem. Solid-State Lett. **10**(10), J120–J122 (2007).

1. Introduction

Colloidal quantum dots (CQDs) are a promising material for use in high efficiency, low-cost photovoltaics due to their size-effect tuneability and compatibility with solution-based deposition. The fact that their bandgap can be easily tuned from 700nm to beyond 1800nm means that they can be used as the absorber material in single junction, tandem, and triple junction photovoltaics.

For many photovoltaic device architectures, it is desirable to deposit a transparent contact on top of a photoactive layer without damaging it. This enables the use of light trapping substrates that could help overcome the transitional absorption/extraction tradeoff faced by all photovoltaic devices [1,2]. It also allows the fabrication of multijunction photovoltaic (PV) devices, and compatibility with the low-cost metal foil substrates [3–5] used in roll-to-roll printing-based deposition processes for single-junction devices.

We present herein an investigation of the impact of transparent top contact deposition on the performance of TiO_2/PbS depleted heterojunction photovoltaic devices. By measuring the efficiency of photocarrier extraction of our devices as a function of illumination wavelength, during either top or bottom illumination, and comparing it with that expected from a simple model of the carrier generation and extraction in such a device, we are able to infer the presence of a substantial 'dead zone', where absorption remains strong but carrier extraction is limited. Such a dead zone has important implications for device design, especially devices where illumination through the top contact is required.

2. Experimental details

Nanocrystal Synthesis. All chemicals were used as-received unless stated otherwise. TMS (0.18 g, 1 mol) was added to 1-Octadecene (10 mL), which had been dried and degassed by heating to 80 °C under vacuum for 24 hours. A mixture of oleic acid (1.34 g, 4.8 mmol), PbO (0.45 g, 2.0 mmol), and 1-Octadecene (14.2 g, 56.2 mmol) was heated to 95 °C under vacuum for 16 hours then placed under Ar. The flask temperature was increased to 125 °C and the TMS/Octadecene mixture was injected. After injection, the temperature dropped to ~95 °C, and the flask was allowed to cool gradually to 36°C.

The nanocrystals were precipitated with 50 mL of distilled Acetone and centrifuged. After discarding the supernatant, the precipitate was redispersed in Toluene. The nanocrystals were precipitated again with 20 mL of Acetone, centrifuged for 5 min, dried, and finally dispersed in toluene (~350 mg mL-1).

Nanocrystals were then precipitated with methanol and dried under vacuum once the supernatant was removed. They were then redispersed in toluene to a concentration of 100mg/ml. This process was repeated twice more, with the final redispersion in octane at a concentration of 50mg/ml.

Electrode Fabrication. TiO_2 nanoparticles, 10-30nm diameter and dispersed in terpineol (DSL90-T, Dyesol) were diluted in either terpineol or ethanol and spin-coated onto Fluorine-dope Tin Oxide (Pilkington TEC15, Hartford Glass) substrates. The nanoparticles were diluted with terpineol (1:3 by weight), spun at 1500rpm, and placed on a hotplate pre-heated to 120 °C. Substrates were then heated at 200 °C for 15 minutes and 400 °C for 60 minutes. Substrates underwent $TiCl_4$ treatment in a 60 mM solution in deionized (DI) water at 70 °C for 30 minutes. Substrates were removed, rinsed with DI water, and fired at 520 °C for 60 minutes. Aside from top contact deposition, all other fabrication was carried out in a fume hood in air ambient.

Device Fabrication. PbS CQDs at 50 mg/ml in octane were applied to the substrates in a layer-by-layer fashion. Two drops of CQDs were dispensed onto the substrate through a 0.2 μm filter and spun at 2500 rpm for 25 seconds. 5 drops of a 10% mercapto propionic acid (MPA)/Methanol solution were applied, and the substrate was spun again. Four rinse steps,

#131000 - $15.00 USD Received 1 Jul 2010; revised 27 Aug 2010; accepted 27 Aug 2010; published 1 Sep 2010

two with MeOH and two with octane, were applied, and the process was repeated until the desired film thickness had been reached.

Indium tin oxide (ITO) top contacts were deposited by DC sputtering in an inert argon environment at room temperature. The chamber was first pumped to a base pressure of 1×10^{-5} Torr, and then worked at a pressure of 5 mTorr for DC sputtering. The 50nm thick ITO film was deposited at a power of 30 W and rate of 0.04 nm/s.

Device Characterization. External quantum efficiency measurements used a Xenon arc lamp coupled to a Jobin Yvon Triax 320 monochromator to provide monochromatic illumination with a 40 nm bandwidth.

Current-voltage measurements used a 975 nm diode laser from QPhotonics connected to a Newport laser diode driver, while bias was applied and current measured using a Keithley 2400 digital multimeter.

3. Results

To determine whether the PbS CQD layer of our devices is damaged during top contact deposition, devices with both top (ITO) and bottom (FTO) transparent contacts were fabricated as described above. Figure 1(a) is a cross sectional scanning electron microscope (SEM) image of a representative device prior to top contact deposition. For such a depleted heterojunction device [6], the electrical band diagram is shown in Fig. 1(b). In general, the portion of the PbS film that is closest to the interface with TiO_2 will be depleted of majority carriers, creating a space charge region where extraction is most efficient due to the presence of a built-in electrical field. If the PbS film is sufficiently thick, or its doping sufficiently high, there will also be a portion that is not fully depleted. The efficiency of carrier extraction from this quasi-neutral region has been shown to be significantly lower than that in the depletion region, due to the reliance on relatively slow and spatially random minority carrier diffusion [7–11]. In this study, we investigated the presence of a third region, which we will refer to as a dead zone, where carrier extraction is significantly reduced. The reason for this reduced extraction efficiency, which could be the presence of a large number of mid-gap trap states (likely due to damage during top contact deposition [12,13]) leading to rapid recombination of photogenerated electrons with (majority carrier) holes, will be the subject of future investigations. Figure 1(c) shows the expected internal quantum efficiency (IQE) in the PbS layer, as a function of distance form the PbS/TiO2 interface, of three devices of varying thickness. Carriers within the depletion region are expected to be swept out efficiently, such that carrier collection is independent of position within this portion of the device. Collection

#131000 - $15.00 USD Received 1 Jul 2010; revised 27 Aug 2010; accepted 27 Aug 2010; published 1 Sep 2010

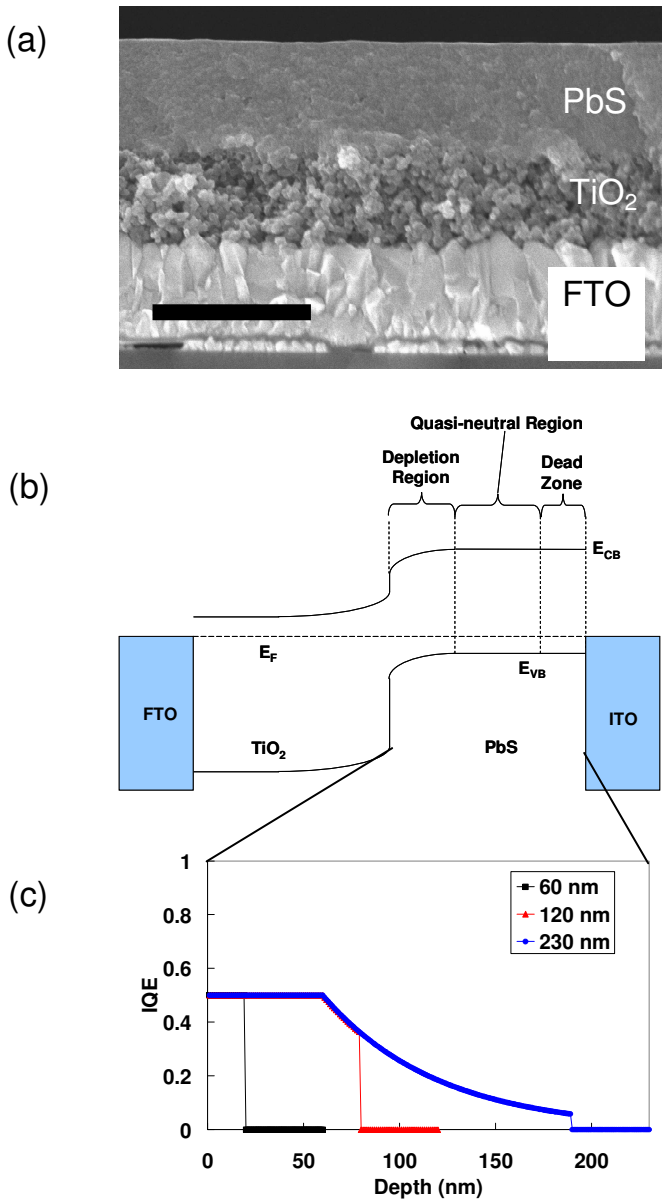

Fig. 1. (a) Cross-sectional SEM image of a device prior to top contact deposition. The scale bar (bottom left) is 500 nm. (b) Electron energy band diagram of a depleted heterojunction (DH) device. (c) Internal quantum efficiency profile in the PbS layer for three DH devices with PbS thicknesses of 60nm, 120nm, and 230nm.

from the remainder of the device is dependent upon diffusion, which we approximate by an exponential dependence on distance from the depletion region edge. For each device, it will be shown that a dead zone is present at the top (ITO) contact. Within this deadzone, carrier collection is negligible, possibly due to the presence of a large number of recombination centers. As the thickness is decreased, the dead zone begins to intrude on the quasi-neutral region and eventually the depletion region, at which point it is shown to have a catastrophic effect on carrier extraction in the device.

To investigate this phenomenon, we performed external quantum efficiency (EQE) measurements, as a function of illumination wavelength, when illuminating from either the

#131000 - $15.00 USD Received 1 Jul 2010; revised 27 Aug 2010; accepted 27 Aug 2010; published 1 Sep 2010

top or bottom of the device. By first measuring the absorption coefficient of our PbS film, and modeling the reflection at the interfaces by assuming dielectric constants of 2.5, 2.8, and 2.0 for the PbS CQD, TiO_2 and ITO layers, respectively, we were able to generate an expected carrier generation profile in our films for top and bottom illumination (Fig. 2). Since short wavelengths are absorbed fairly strongly in our devices, while longer wavelengths penetrate deeper into the device, the spectral EQE shape for top and bottom illumination can be a sensitive indicator of the collection efficiency as a function of position in our device. Figure 3 shows the measured external quantum efficiency of three devices, with PbS thicknesses of 60nm [Fig. 3(a)], 120nm [Fig. 3(b)], and 230nm [Fig. 3(c)], respectively, for top vs. bottom illumination. In each case the EQE for infrared (IR) wavelengths, where absorption is weak and the carrier generation rate is therefore relatively constant as a function of distance from the PbS/TiO_2 interface, is similar for top and bottom illumination. For visible wavelengths the EQE is lower when the device is illuminated from the top. This is expected for the thickest device, where there is likely to be a quasi-neutral region, with its associated lower photogenerated charge carrier extraction efficiency, far from the PbS/TiO_2 interface. However, even for the 60nm device, which should be fully depleted, there is some deviation in EQE below 550nm.

To calculate the EQE spectrum for the devices, we used our approximation of the carrier generation profile, together with the internal quantum efficiency profiles shown in Fig. 1(c), to calculate the contribution to the EQE, per unit length, in each region of the device. These EQE density plots are shown in Fig. 4 for both top and bottom illumination. The EQE spectrum is then calculated by integrating over the entire PbS layer. Figure 3(d) and 3(e) show the calculated expected EQE spectra, for top and bottom illumination, for the three device thicknesses mentioned above. Agreement between the calculated and measured spectra was obtained by varying the width of the depletion region, quasi-neutral region, and dead zone. It was found that a semi-quantitative agreement between the calculated and measured spectra could only be obtained when a sizeable dead zone (40nm for the plots shown) was included. Shrinking the depletion region was insufficient, as it could not

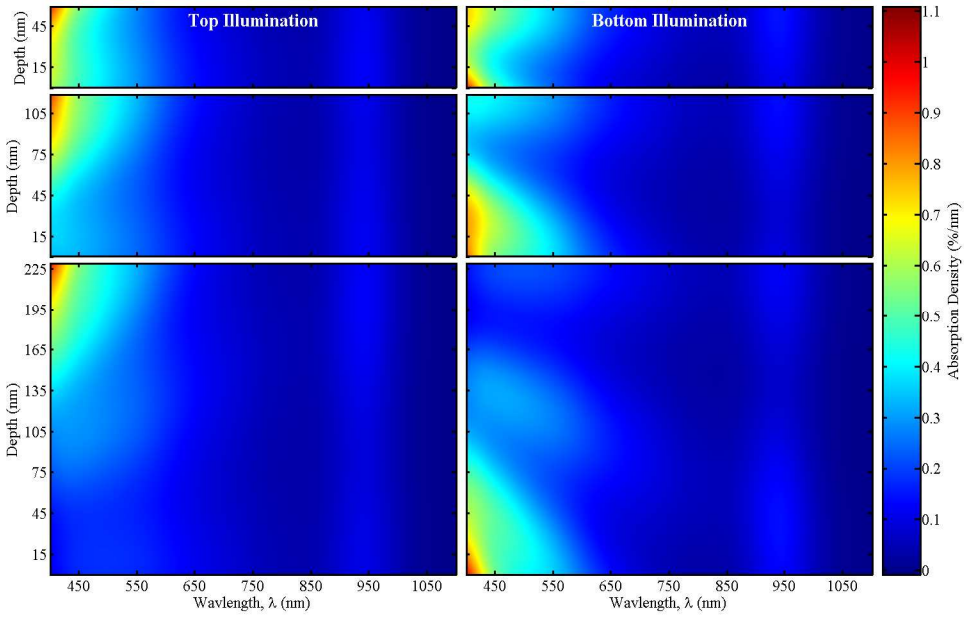

Fig. 2. Carrier generation profile in the PbS layer of an $FTO/TiO_2/PbS$ CQD/ITO device that is 60 (top), 120 (middle), or 230 (bottom) nm thick, illuminated from the top (left) or bottom (right).

#131000 - $15.00 USD Received 1 Jul 2010; revised 27 Aug 2010; accepted 27 Aug 2010; published 1 Sep 2010

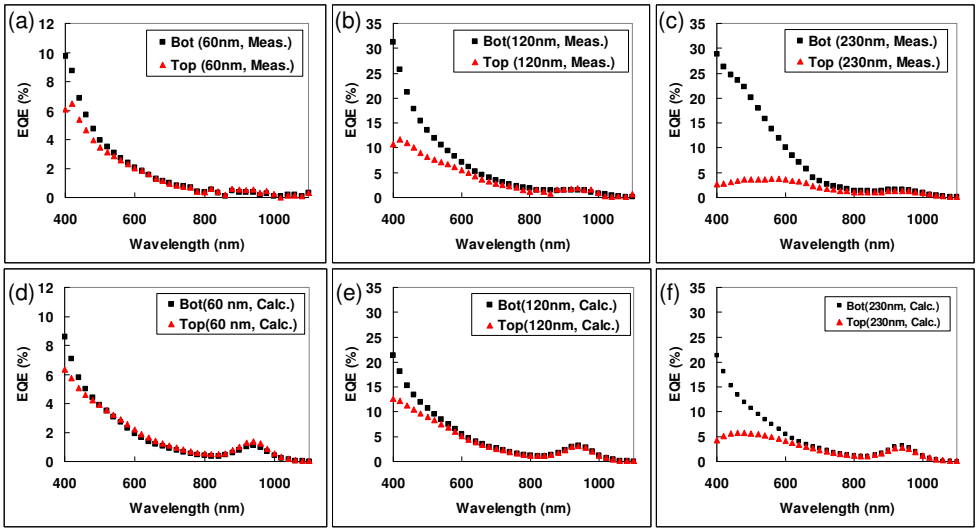

Fig. 3. Measured (a-c) and calculated (d-f) EQE spectra, for illumination from either the top or bottom, for devices with PbS layers that are 60nm (a,d), 120nm (b,e), and 230nm (c,f) thick. The fitting parameters were: depletion width: 50nm, diffusion length: 10nm, dead zone width: 40nm, IQE: 0.5.

reproduce the significant disparity between top and bottom illumination for the 60nm device without drastically reducing the EQE values obtained for the thicker devices. It is therefore believed that there is significant damage to the upper region of these devices, most likely due to sputtering-induced damage of the PbS layer producing a significant number of mid-gap traps.

To determine whether this insight could be used to improve the performance of our devices, we deposited a thin (2nm) layer of Au on top of our PbS film by thermal evaporation prior to sputtering of ITO. As we can see in Fig. 5, which shows the I-V curve under

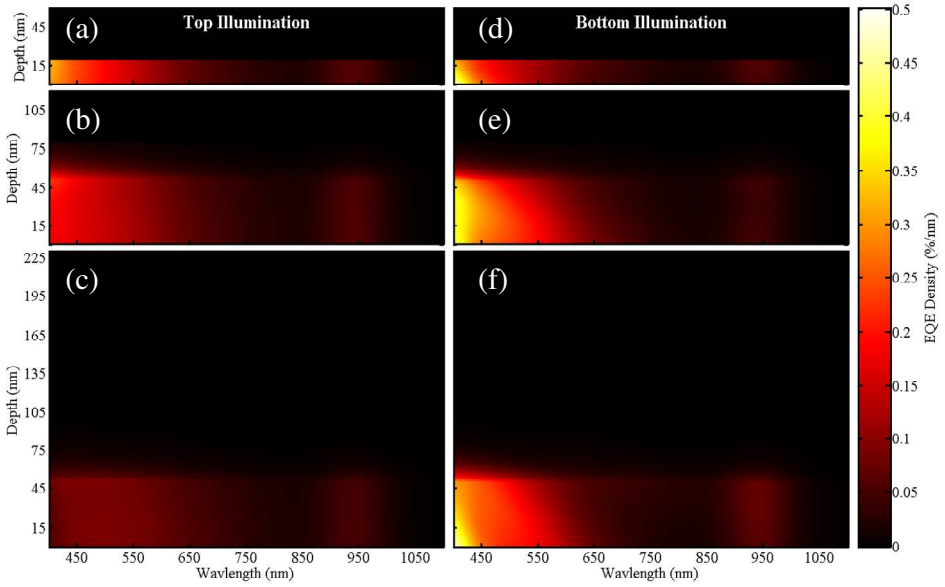

Fig. 4. Carrier extraction profile for top (a-c) and bottom (d-f) illumination, for devices with a PbS layer that is 60nm (a,d), 120nm (b,e), or 230nm (c,f) thick. The devices have a depletion width of 60nm, diffusion length of 10nm, dead zone width of 40nm, and an IQE of 0.5.

#131000 - $15.00 USD Received 1 Jul 2010; revised 27 Aug 2010; accepted 27 Aug 2010; published 1 Sep 2010

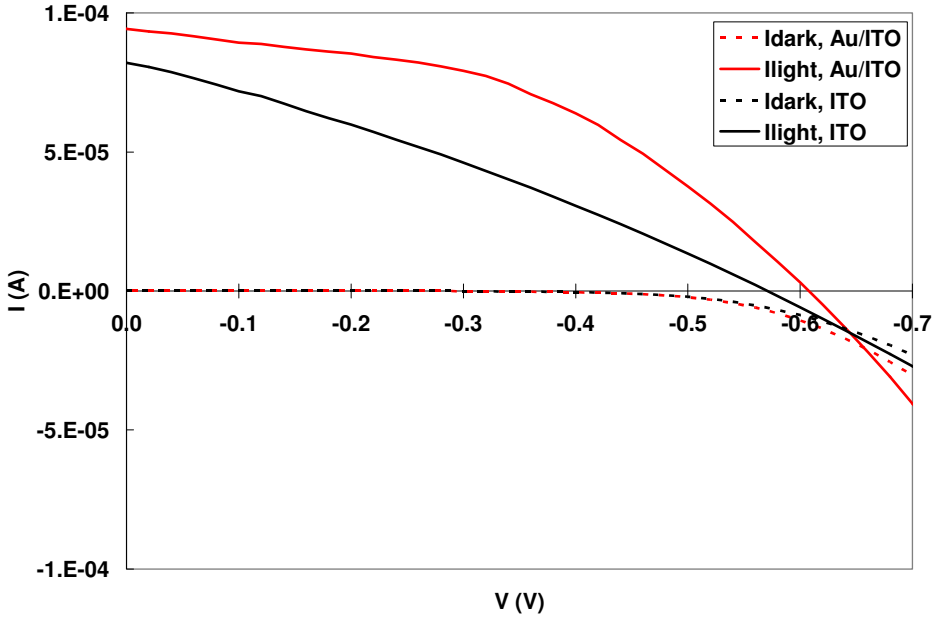

Fig. 5. I-V curves of FTO/TiO_2/PbS CQD/(ITO or Au/ITO) devices under 975nm illumination at 100 mW/cm^2.

975nm illumination device with and without a layer of Au between the ITO and PbS, the device performance is increased due to an increase in the series resistance and a decrease in the shunt resistance, as inferred by the slope of the I-V curves as they cross the voltage and current axes, respectively. Such an increase is encouraging, but a 2nm Au layer is unlikely to fully protect the underlying PbS layer, and a thicker layer ceases to be sufficiently transparent to allow illumination from the top. While it is likely that the film is damaged due to the harsh conditions during ITO deposition (Argon ion/atom bombardment, UV illumination from the plasma, heating or ballistic damage from the sputtered ITO particles, etc.), further investigation is required in order to better understand the nature of this damage and its cause. If this is the cause of the dead zone formation in these devices, it is believed that the inclusion of an optically transparent hole transport layer between the PbS and ITO may help reduce the damage incurred by the PbS during deposition.

4. Conclusion

Spectral EQE measurements, obtained by illuminating through either the top or bottom contact of a FTO/TiO_2/PbS CQD/ITO photovoltaic device, are shown to be a sensitive indicator of collection efficiency as a function of position in the device. By comparing these spectra with spectra calculated using the estimated carrier generation profile in our devices, together with reasonable values of IQE, depletion width, and diffusion length, it was found that a large 'dead zone' must be present at the top of the devices, just under the ITO contact. Such a dead zone would cause a catastrophic loss of efficiency for devices that are illuminated through this top contact. The origins of this damaged region in the device, and possible means of preventing its formation, will be the subject of future investigations.

Acknowledgement

This publication was supported in part by King Abdullah University of Science and Technology (KAUST), Award No. KUS-I1-009-21.

#131000 - $15.00 USD Received 1 Jul 2010; revised 27 Aug 2010; accepted 27 Aug 2010; published 1 Sep 2010